Slow light based on population oscillation in quantum dots with inhomogeneous broadening

Shu-Wei Chang and Shun Lien Chuang*
Department of Electrical and Computer Engineering, University of Illinois at Urbana-Champaign, Illinois 61801, USA
(Received 18 August 2005; revised manuscript received 6 October 2005; published 22 December 2005)

We propose using population oscillation in a quantum-dot absorptive medium to demonstrate a potential slow-light device. The confinement potential of quantum dots leads to discrete electronic density of states, of which the first electron and hole quantized states form the two-level system for population oscillation. The optical pump creates a coherent absorption dip centered at the pump frequency, even though not all the quantum dots are in resonance with the pump due to inhomogeneous size distribution. Thus, the inhomogeneous broadening of quantum dots will not wash out the effect of population oscillation. Under a typical dot surface density of 10^{10} cm^{-2}, a slowdown factor of several hundreds is possible for a normal incidence geometry.

DOI: 10.1103/PhysRevB.72.235330 PACS number(s): 78.67.Hc, 71.35.Gg, 73.21.La, 78.20.Ci

I. INTRODUCTION

In a dispersive medium, if a positive-slope variation of the real part of the refractive index with respect to frequency is steep within a narrow frequency range, the group velocity of a wave packet with frequency components within this frequency range can be considerably reduced. Significant slowdown of light pulses with a slowdown factor of about 10^7 has been achieved by electromagnetically induced transparency (EIT) using atomic vapors at a low temperature.[1] Despite a huge slowdown factor, EIT requires a long optical decoherence time. Such a long timescale for optical dipole interactions is usually difficult to maintain at room temperature. Instead of optical decoherence time, other timescales which remain long at room temperature are utilized to produce steep variations of the real part of the refractive index, e.g., the coherent population oscillation (PO) using population relaxation lifetime,[2,3] spin-dependent EIT using spin lifetime,[4] and a grating effect using the grating response time of a photorefractive medium.[5] Pump-probe experiments are then used to sense these long time scales corresponding to different mechanisms via optical dipole interactions within the media. These long time scales create a sharp small-signal absorption dip or gain peak for the probe signal with a narrow linewidth inversely proportional to the time scales. From Kramers-Kronig (KK) relations, a steep variation with a positive slope corresponding to the sharp absorption dip or gain peak is present on the spectrum of the real part of the refractive index and can be utilized for slow light.

Slow-light devices using semiconductor nanostructures are of great interest because they can be potentially integrated with other components in an optical communication system. Among all the possible mechanisms for slow-light phenomena in semiconductors, excitonic PO in quantum wells (QWs) has been successfully demonstrated at a low temperature.[3,6] The same idea can be applied to quantum dots (QDs). The prominent advantage of QDs originates from their three-dimensional confinement potential which localizes the electron-hole pairs in the same dot. First, in the absorptive regime, population inversion for most of QD states is not reached. The transfer of electrons or holes from ground states to excited states and wetting layer states is slower than the corresponding carrier transfer in QWs due to the discrete density of states and absence of intradot carrier-carrier scattering. Thus, the insensitivity of QW excitons to the optical dipole interaction due to the scattering from a state with a lower center-of-mass momentum to another with a higher center-of-mass momentum can be avoided. Second, even though the attractive Coulomb potential is screened, the electron-hole pair still remains in the same dot because of the three-dimensional confinement potential of QDs. The energy of the electron-hole pair may be slightly changed because of screening of the Coulomb interaction, but the corresponding oscillator strength will not be changed much. Thus, the excitonic nature of the two-level system used in PO plays a less significant role for QDs. It is possible for PO to be present at room temperature even though it is electron-hole pairs rather than excitons which are responsible for this coherent process.

An important advantage to use PO in QDs as a potential slow-light device is the immunity to inhomogeneous broadening. Inhomogeneous broadening is an undesired factor limiting the performance of a QD laser. In view of slow-light devices, the slowdown factor will be significantly lowered if the sharp absorption dip or gain peak resulting from these long time scales are washed out by the fluctuation of the energy levels. Slow light using typical Λ-type or ladder-type EIT in QDs with inhomogeneous broadening suffers from this problem.[7] Mechanisms insensitive to the fluctuation of energy levels such as EIT based on V system with near-degenerate excited states using spin-based scheme[4] may be used. On the other hand, the position of the coherent dip from PO on the absorption spectrum is only determined by the pump frequency. The depths of the individual absorption dip may be different for distinct QDs, but they all occur at the same frequency and add up constructively. Thus, the slowdown effect is not washed out by inhomogeneous broadening because each dip on the absorption spectrum is centered at the pump frequency, and its position is not influenced by the transition frequency of the corresponding QD.

In this paper, we model excitonic PO in QDs using a variational approach. For each QD size, the corresponding

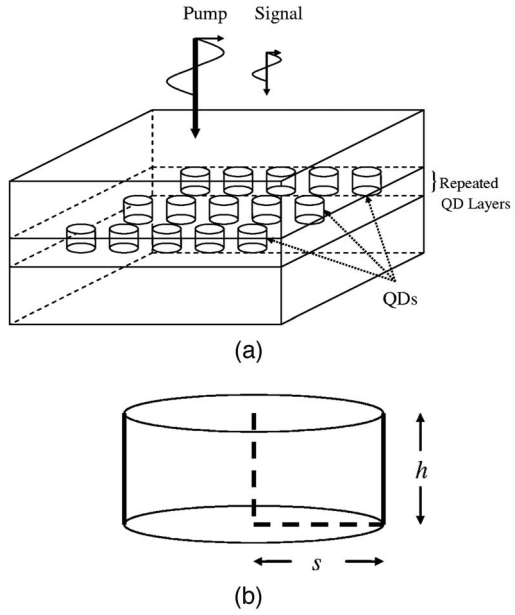

FIG. 1. (a) The pump-probe scheme of population oscillation in QDs. Both the pump and signal are incident normally to QD layers. (b) The geometry of a QD. The QD is modeled as a disk with height h and radius s.

energy level and dipole moment of the excitonic ground state are calculated by adjusting the variational wave function. The ensemble sum of dipole moments will be carried out by modeling the size fluctuation as a Gaussian distribution. The calculated absorption spectrum exhibits two different characteristics. One is the wide spectral hole burning with a linewidth of a few millielectron volts. The other is the narrow coherent dip characterized by the population lifetime of the electron-hole pair. We assume low-temperature operation since the wide spectral hole burning caused by the continuous-wave pump can only be observed if the redistribution of the carriers among all the QDs is not fast enough to fill out the spectral hole.[8–11] Using a normal incidence geometry, a slowdown factor of about several hundreds can be achieved for a typical QD areal density.

II. POPULATION OSCILLATION IN QUANTUM DOTS

As shown in Fig. 1, we consider a pump-probe scheme in which a pump and signal are incident along the direction normal to the wetting layer. QDs are uniformly distributed in the plane parallel to the wetting layer. The geometry of a QD is a disk with height h and radius s. We include the effect of inhomogeneous broadening by treating the radius s of a QD as a random variable with a Gaussian distribution. Although the fluctuation of the QD height h is also present, we simply set it to a constant because it merely introduces a more complicated inhomogeneous-broadened line shape without altering the basic physics.

For a given QD size, we consider the pump-probe scheme which probes the transition of the exciton state formed by the heavy hole (HH)-like and conduction-band ground states. Without the band-mixing effect, the effective-mass Hamiltonian of a HH-like exciton in a quantum disk can be written as

$$H_{eh} = \frac{P_{z_e}\gamma_c(\mathbf{r}_e)P_{z_e}}{2m_0} + \frac{P_{z_h}[\gamma_1(\mathbf{r}_h) - 2\gamma_2(\mathbf{r}_h)]P_{z_h}}{2m_0} + \frac{\mathbf{P}_{\perp,e}\cdot\gamma_c(\mathbf{r}_e)\mathbf{P}_{\perp,e}}{2m_0} + \frac{\mathbf{P}_{\perp,h}\cdot[\gamma_1(\mathbf{r}_h) + \gamma_2(\mathbf{r}_h)]\mathbf{P}_{\perp,h}}{2m_0} + V_e(\mathbf{r}_e) + V_h(\mathbf{r}_h) + E_{g,B} - \frac{e^2}{4\pi\epsilon}\frac{1}{|\boldsymbol{\rho}_e - \boldsymbol{\rho}_h|}, \quad (1)$$

where $\gamma_c(\mathbf{r}_e)$ is the position-dependent inverse effective mass in the conduction band; $\gamma_1(\mathbf{r}_h)$ and $\gamma_2(\mathbf{r}_h)$ are position-dependent Luttinger's parameters; $V_e(\mathbf{r}_e)$ and $V_h(\mathbf{r}_h)$ are the confinement potentials of electrons and holes, respectively; $E_{g,B}$ is the difference between conduction and valence band edges; ϵ is the dielectric constant of the material; and $\boldsymbol{\rho}_e$ and $\boldsymbol{\rho}_h$ are the electron and hole coordinates perpendicular to the growth direction. The origin of the coordinate system is located at the center of the QD. In Eq. (1), the zero energies of electrons and holes are set at the respective barrier band edges. In this way, the band edge difference $E_{g,B}$ in the barrier region is added to account for the energy of the optical transition.

We construct the variational envelope function of this HH-like exciton using the method of separation of variables. The variational envelope function is written as

$$\Psi_{ex}(\mathbf{r}_e,\mathbf{r}_h) = \varphi_e(z_e)\psi_e(\rho_e)\varphi_h(z_h)\psi_h(\rho_h),$$

$$\psi_{e(h)}(\rho_{e(h)}) = A(\lambda_{e(h)})\left(\rho_{e(h)} + \frac{s}{\lambda_{e(h)}}\right)\exp\left(-\lambda_{e(h)}\frac{\rho_{e(h)}}{s}\right), \quad (2)$$

where λ_e and λ_h are dimensionless variational parameters of the in-plane trial envelope function $\psi_e(\rho_e)$ and $\psi_h(\rho_h)$ for electron and hole components; A is the in-plane normalization constant; and $\varphi_e(z_e)$ as well as $\varphi_h(z_h)$ are the envelope functions along the growth direction and can be explicitly expressed as

$$\varphi_e(z_e) = \begin{cases} A_{z,e}\cos(k_e z_e), & |z_e| \leq \dfrac{h}{2}, \\ B_{z,e}\exp(-\nu_e|z_e|), & |z_e| > \dfrac{h}{2}, \end{cases}$$

$$B_{z,e} = A_{z,e}\cos(k_e z_e)\exp\left(\frac{\nu_e h}{2}\right),$$

$$\varphi_h(z_h) = \begin{cases} A_{z,h}\cos(k_h z_h), & |z_h| \leq \dfrac{h}{2}, \\ B_{z,h}\exp(-\nu_h|z_h|), & |z_h| > \dfrac{h}{2}, \end{cases}$$

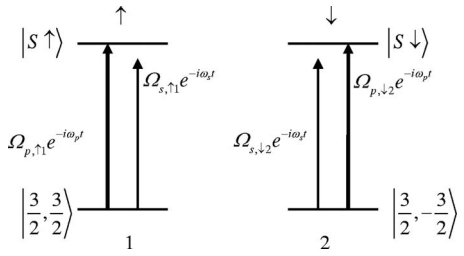

FIG. 2. The energy levels, the pump, and the signal of a spin-up and spin-down exciton in a QD.

$$B_{z,h} = A_{z,h}\cos(k_h z_h)\exp\left(\frac{\nu_h h}{2}\right), \tag{3}$$

where $A_{z,e}$, $B_{z,e}$ are the normalization constants for the electron enevelope function $\varphi_e(z_e)$, while $A_{z,h}$ and $B_{z,h}$ are the normalization constants for the hole envelope function $\varphi_h(z_h)$; and k_e as well as ν_e are the parameters describing the oscillatory and decaying behaviors of the electron envelope function $\varphi_e(z_e)$, while k_h as well as ν_h are the corresponding counterparts of the hole envelope function $\varphi_e(z_e)$. The form of the variational wave function on the second line of Eq. (2) is commonly used in the calculation of the ground state energy of a helium 4 atom and can be found in many standard textbooks, e.g., see Ref. 12. However, unlike the ground state of a two-dimensional hydrogen atom, a term linear in the electron (hole) radius $\rho_e(\rho_h)$ is added. The presence of this term is due to the requirement of a zero gradient at the origins of the in-plane coordinates $\boldsymbol{\rho}_e$ and $\boldsymbol{\rho}_h$

$$\nabla_{\perp,e}\Psi_{ex}(\mathbf{r}_e,\mathbf{r}_h)_{\boldsymbol{\rho}_e=\boldsymbol{\rho}_h=\mathbf{0}} = \nabla_{\perp,h}\Psi_{ex}(\mathbf{r}_e,\mathbf{r}_h)_{\boldsymbol{\rho}_e=\boldsymbol{\rho}_h=\mathbf{0}} = \mathbf{0}. \tag{4}$$

Since the QD confinement potential is nonsingular, the electron and hole components of the variational wave function should be smooth at the corresponding origins, just like the fundamental guided mode of an optical fiber. Using Eqs. (2) and (3), we then calculate the expectation value $\langle\Psi_{ex}|H_{eh}|\Psi_{ex}\rangle$ and minimize it with respect to the parameters λ_e and λ_h. The detailed derivation of this expectation value $\langle\Psi_{ex}|H_{eh}|\Psi_{ex}\rangle$ will be given in Appendix A.

From the variational wave function $\Psi_{ex}(\mathbf{r}_e,\mathbf{r}_h)$, we can calculate the dipole moment and, thus, the corresponding Rabi frequency used in the density-matrix formalism. For an arbitrary QD, the energy levels of the ground-state exciton and the optical transitions caused by the pump and signal are shown in Fig. 2. Two conduction bands (↑ and ↓) and two heavy-hole (HH) bands ($1 \equiv |3/2,3/2\rangle$ and $2 \equiv |3/2,-3/2\rangle$) are used. Although band mixing may lead to a complicated hole structure for these exciton systems, it is possible to make the hole part of the ground exciton wave function HH-like by compressive strain.[13] The dynamic equations of the corresponding density matrix elements in the two-level approximation are written as

$$\begin{aligned}
\partial_t N_\uparrow &= -\gamma(N_\uparrow - N_\uparrow^{(0)}) - \gamma_s(N_\uparrow - N_\downarrow) \\
&\quad + i[\Omega_{\uparrow 1}(t)P_{1\uparrow} - P_{\uparrow 1}\Omega_{1\uparrow}(t)], \\
\partial_t N_\downarrow &= -\gamma(N_\downarrow - N_\downarrow^{(0)}) - \gamma_s(N_\downarrow - N_\uparrow) \\
&\quad + i[\Omega_{\downarrow 2}(t)P_{2\downarrow} - P_{\downarrow 2}\Omega_{2\downarrow}(t)], \\
\partial_t N_1 &= \gamma(N_\uparrow - N_\uparrow^{(0)}) - \Gamma_s(N_1 - N_2) + i[\Omega_{1\uparrow}(t)P_{\uparrow 1} - P_{1\uparrow}\Omega_{\uparrow 1}(t)], \\
\partial_t N_2 &= \gamma(N_\downarrow - N_\downarrow^{(0)}) - \Gamma_s(N_2 - N_1) + i[\Omega_{2\downarrow}(t)P_{\downarrow 2} - P_{2\downarrow}\Omega_{\downarrow 2}(t)], \\
\partial_t P_{\uparrow 1} &= -i[\omega_{ex} - i\Gamma_2(N_\uparrow - N_1, N_\downarrow - N_2)]P_{\uparrow 1} \\
&\quad - i\Omega_{\uparrow 1}(t)(N_\uparrow - N_1), \\
\partial_t P_{\downarrow 2} &= -i[\omega_{ex} - i\Gamma_2(N_\uparrow - N_1, N_\downarrow - N_2)]P_{\downarrow 2} \\
&\quad - i\Omega_{\downarrow 2}(t)(N_\downarrow - N_2), \\
2 &= N_\uparrow^{(0)} + N_\downarrow^{(0)} + N_1^{(0)} + N_2^{(0)},
\end{aligned} \tag{5}$$

where $N_\uparrow$, $N_\downarrow$, N_1, and N_2 are the respective populations in the conduction bands $|S\uparrow\rangle$ and $|S\downarrow\rangle$ as well as the valence bands $|3/2,3/2\rangle$ and $|3/2,-3/2\rangle$ while $N_\uparrow^{(0)}$, $N_\downarrow^{(0)}$, $N_1^{(0)}$, and $N_2^{(0)}$ are the corresponding counterparts in the absence of pump and signal; $P_{\uparrow 1}$ and $P_{\downarrow 2}$ are the polarizations induced by the pump and signal; γ is the inverse of the population lifetime in states $|\uparrow\rangle$ and $|\downarrow\rangle$; γ_s and Γ_s are the spin-flip constants of the conduction and valence bands; $\Gamma_2(N_\uparrow - N_1, N_\downarrow - N_2)$ is the population-dependent dephasing constant due to excitation induced dephasing (EID);[14] ω_{ex} is the transition frequency of the exciton; and $\Omega_{\uparrow 1}(t)$ and $\Omega_{\downarrow 2}(t)$ are the time-dependent Rabi frequencies which induce the transitions between components ↑ and 1 as well as between components ↓ and 2. On the last line of Eq. (5), we use the conservation of the population in various components, which is a characteristic of a closed system and should be a good approximation at low temperatures. Also, the dephasing constant $\Gamma_2(N_\uparrow - N_1, N_\downarrow - N_2)$ due to EID is modeled as a linear relationship of various populations[14]

$$\begin{aligned}
\Gamma_2(N_\uparrow - N_2, N_\downarrow - N_1) &\sim \Gamma_2^{(0)} + \gamma_2[(N_\uparrow - N_2) + (N_\downarrow - N_1) \\
&\quad - (N_\uparrow^{(0)} - N_2^{(0)}) - (N_\downarrow^{(0)} - N_1^{(0)})],
\end{aligned} \tag{6}$$

where $\Gamma_2^{(0)}$ is the intrinsic dephasing constant; and γ_2 is the proportional constant describing EID. The time-dependent Rabi frequencies $\Omega_{\uparrow 1}(t)$ and $\Omega_{\downarrow 2}(t)$ are composed of the pump and signal components as follows

$$\begin{aligned}
\Omega_{\uparrow 1}(t) &= \Omega_{s,\uparrow 1}e^{-i\omega_s t} + \Omega_{p,\uparrow 1}e^{-i\omega_p t} \\
\Omega_{\downarrow 2}(t) &= \Omega_{s,\downarrow 1}e^{-i\omega_s t} + \Omega_{p,\downarrow 1}e^{-i\omega_p t} \\
|\Omega_{p,\uparrow 1}| &= |\Omega_{p,\downarrow 1}| = \frac{|I_{ch}er_{ch}E_p|}{2\sqrt{2}\hbar}, \\
|\Omega_{s,\uparrow 1}| &= |\Omega_{s,\downarrow 1}| = \frac{|I_{ch}er_{ch}E_s|}{2\sqrt{2}\hbar},
\end{aligned} \tag{7}$$

where er_{ch} is the interband dipole moment; E_p and E_s are the optical fields of the pump and signal; and I_{ch} is the wave function overlap of the electron and hole components in the variational wave function of the exciton

$$I_{ch} = \int_{-\infty}^{\infty} dz \varphi_e(z)\varphi_h(z) \int d\boldsymbol{\rho}\psi_e(\boldsymbol{\rho})\psi_h(\boldsymbol{\rho}). \quad (8)$$

The expression of the overlap integral I_{ch} is shown in Appendix A.

The above equations are aimed at a particular QD. We are interested in the linear relative permittivity tensor $\bar{\bar{\epsilon}}_s^L(\omega_s)$ of the signal. The linear relative permittivity tensor is obtained from the sum of the individual polarization of each QD since the linear electric displacement is an extensive quantity. For a particular QD, the derivation of the corresponding contribution to the total linear permittivity follows an analogous approach in Ref. 6. The main idea is to find the stationary populations of these energy levels and the corresponding background absorption saturated by the pump. Linearized equations corresponding to the beating of the populations in various energy levels and the polarizations induced by the signal can then be derived via the perturbation theory. The absorption and dispersion of the signal are then obtained from the signal polarizations. A similar approach using a systematic perturbation theory but with a different concern on the four-wave mixing in QD gain media can be found in Ref. 15. The detailed expression of the permittivity function as a sum of the contributions from all the QDs will be presented in Appendix B. This summation can be approximated by an integral over the radius s. For a given radius s, denote the linear relative susceptibilities experienced by the signal with polarizations parallel and orthogonal to that of the pump as $\chi_x(\omega_s,s)$ and $\chi_y(\omega_s,s)$, respectively. In the infinitesimal interval ds, the number of QDs dN_{QD} with radius ranging from s to $s+ds$ is

$$dN_{QD} = N_d f(s) ds, \quad (9)$$

where N_d is the *total* number of QDs. The relative linear permittivity tensor $\bar{\bar{\epsilon}}_s^L(\omega_s)$ experienced by the signal can then be approximated by an integral

$$\begin{aligned}\bar{\bar{\epsilon}}_s^L(\omega_s) &= \begin{pmatrix} \epsilon_{bgd} & 0 \\ 0 & \epsilon_{bgd} \end{pmatrix} \\ &\quad + \int ds N_d f(s) \frac{\pi s^2}{A} \begin{pmatrix} \chi_x(\omega_s,s) & 0 \\ 0 & \chi_y(\omega_s,s) \end{pmatrix} \\ &= \begin{pmatrix} \epsilon_{bgd} & 0 \\ 0 & \epsilon_{bgd} \end{pmatrix} \\ &\quad + n_d \pi \int ds f(s) s^2 \begin{pmatrix} \chi_x(\omega_s,s) & 0 \\ 0 & \chi_y(\omega_s,s) \end{pmatrix}, \quad (10)\end{aligned}$$

where $n_d = N_d/A$ is the surface density of QDs. The probability distribution function $f(s)$ is modeled as a Gaussian distribution

$$f(s) = \frac{1}{\sigma_s \sqrt{2\pi}} \exp\left[-\frac{(s-\bar{s})^2}{2\sigma_s^2} \right], \quad (11)$$

where $\bar{s}$ is the mean of the QD radius; and σ_s is the standard deviation of the QD radius.

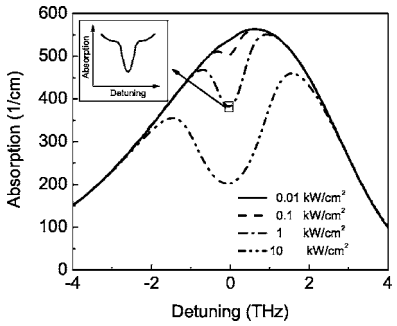

FIG. 3. The global view of the absorption spectrum of an inhomogeneous-broadened QD system. As the pump intensity increases, a broad spectral hole with a linewidth increasing with the pump intensity is present on the absorption spectrum.

III. CALCULATIONS

We consider the system of $In_{0.25}Ga_{0.75}As/GaAs$ QDs. The dot density n_d is set to 10^{10} cm^{-2}. The potential barriers $V_{e,B}$ and $V_{h,B}$ calculated from model-solid theory[16] are 292.7 meV and 72.3 meV, respectively. The inverse of the relative conduction band effective mass $\gamma_{c,b}$ and the two Luttinger parameters $\gamma_{1,b}$ and $\gamma_{2,b}$ in the barrier region are 14.93, 6.8, and 1.9, respectively. Their counterparts $\gamma_{c,d}$, $\gamma_{1,d}$, and $\gamma_{2,d}$ in the QD region are 17.86, 8.03, and 2.43, respectively. The mean QD radius is 80 Å, and the standard deviation of the QD radius is 10 Å. The height of QD h is set to 50 Å. At the mean QD radius, the variational exciton energy is 1294 meV, and the photon energy of the pump is set to this value. The pump intensities are set to 0.01, 0.1, 1, and 10 kW/cm^2. The inverse of the population lifetime γ is set to 2.5 ns^{-1} independent of the QD size. Similarly, the spin-flip constants Γ_s and γ_s are set to 1.25 ns^{-1} and 0.2 ps^{-1}, respectively, which are independent of the QD size. The intrinsic dephasing constant $\Gamma_2^{(0)}$ and the EID constant are set to 1 ps^{-1} and 1.8 ps^{-1}, respectively, for all QDs. We consider only the case of parallel polarizations for which the PO effect is maximal. The PO effect is reduced if the pump and signal polarizations are orthogonal. The refractive index $n_s(\omega_s)$, the absorption $A_s(\omega_s)$, and the slowdown factor $R_s(\omega_s)$ are calculated by the following relations:

$$n_s(\omega_s) = \sqrt{\epsilon_{bgd} + \chi_x(\omega_s)}, \quad A_s(\omega_s) = 2\frac{\omega_s}{c}\mathrm{Im}[n_s(\omega_s)],$$

$$R_s(\omega_s) = \mathrm{Re}[n_s(\omega_s)] + \omega_s \frac{\partial\, \mathrm{Re}[n_s(\omega_s)]}{\partial \omega_s}. \quad (12)$$

Figure 3 shows the absorption spectra over a broad frequency range for different pump intensities. These spectra reflect the inhomogeneous broadening due to the size fluctuation for the transition of the ground state exciton. The full width at half maximum (FWHM) at a low pump intensity (solid curve) is about 4.5 THz (18.3 meV). If the fluctuations of the QD height and composition are taken into account, the inhomogeneous-broadened line shape will be even broader. The line shape in Fig. 3 corresponds to an absorption measurement with a coarse resolution (THz scale). Only the glo-

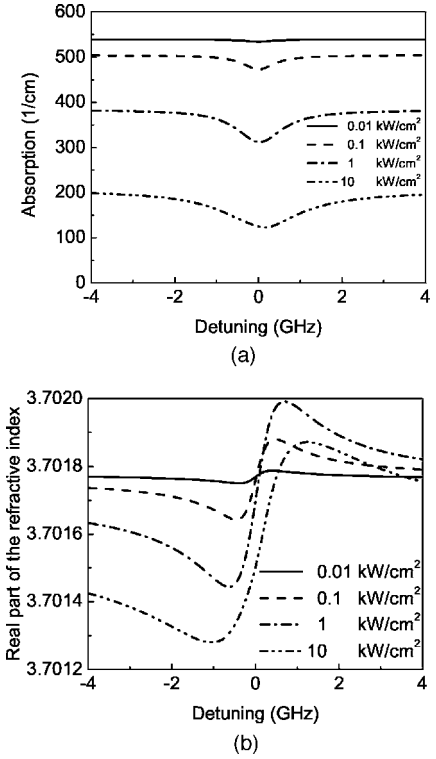

FIG. 4. The local view of the absorption spectrum and the real part of the refractive index as a function of the pump-signal detuning under different pump intensities. (a) As the pump intensity increases, a more significant absorption dip with a FWHM characterized by the inverse of the population lifetime over $2\pi(\gamma/2\pi)$ is present even though the system is inhomogeneous broadened. (b) As the pump intensity increases, the slope of the variation near the pump frequency will first increase and then decrease. There is an optimal intensity at which the slowdown factor is optimized.

bal features of the absorption spectra are resolved (when the resolution is reduced to the GHz scale, the characteristics of PO will be clearer, as indicated by the inset in Fig. 3, and will be addressed in Fig. 4). As the pump intensity increases, a spectral hole with a linewidth increasing with the pump intensity is created on the absorption spectrum. This spectral hole is a characteristic of an inhomogeneous-broadened system[17] because the transitions resonant with the pump frequency are saturated more while those further away from the resonance are less influenced. However, as the pump intensity increases, the transition originally not in resonance with the pump frequency will also be saturated. The saturation of these nonresonant transitions broadens the spectral hole. Thus, the linewidth of this spectral hole reflects a time scale determined by the homogenous linewidth and the pump intensity (the Rabi frequency). Note that in this model, we do not take into account the redistribution of the population between excited states or between different QDs. At high temperatures, the redistribution of the population cannot be neglected, and this broad spectral hole may be reduced significantly if the pump is a *continuous-wave* laser. In that case, one can only obtain a smooth absorption spectrum which is saturated as a whole by the pump in a measurement with a coarse resolution.

Figure 4(a) shows the absorption spectra over a narrow frequency range (GHz scale) for different pump intensities. These absorption spectra correspond to measurements with a fine resolution near the pump frequency. The background absorptions in Fig. 4(a) under different pump intensities are the values at the bottoms of the broad spectral holes in Fig. 3. There are local features present in the absorption spectrum. Coherent absorption dips centered at zero detuning are created. The corresponding half widths at half maximum (HWHMs) are roughly the inverse of the population lifetime over $2\pi(\gamma/2\pi=0.398\ \mathrm{ns}^{-1})$. These absorption dips are due to the PO corresponding to the transition of ground-state exciton from each QD. An interesting point is that this coherent effect can be quite significant even though the QD system is seriously homogeneous broadened. Compared with slow light using EIT in an inhomogeneously-broadened QD system,[7] the contributions to the coherent dip of PO from each QD do not interfere with each other because the spectral position of the individual absorption dip from each QD is the same as the pump frequency. Even if a significant number of transitions are not resonant with the pump frequency, the contributions from all the QDs still add up constructively. Although transitions from the QDs which are not resonant with the pump frequency contribute relatively less, they do not play a role in eliminating the absorption dip from PO. Also, the coherent absorption dip is expected to be observable at room temperature for an inhomogeneous-broadened QD system. Unlike the broad spectral hole in Fig. 3 which may be eliminated by population redistribution under a continuous-wave pump, the coherent absorption dip from the PO in this inhomogeneous-broadened QD system should still be present in the absorption spectrum because of the three-dimensional confinement of the QD potential. As long as there are carriers in QDs, the corresponding beating caused by the pump and signal can always be induced. However, the HWHM of the absorption dip is expected to be larger than that at a low temperature because other mechanisms which are absent at low temperatures can cause the population in a certain QD to vanish. The corresponding loss rate will be reflected on the linewidth of the absorption dip resulted from PO.

Figure 4(b) shows the real part of the refractive index over the same frequency range (GHz) for different pump intensities. From Kramers-Kronig relations, a narrow absorption dip is accompanied by a steep and positive-slope variation in the spectrum of the real part of the refractive index. As shown in Fig. 4(b), the steep changes of the real part of the refractive index take place in the same frequency range of the corresponding absorption dips. In addition to the steep variation, the background of the real part of the refractive index is also shifted as the pump intensity increases. The shift reflects the change of the background absorption. This phenomenon is similar to the variation of the refractive index due to the current injection in a semiconductor laser diode, which is described by the linewidth enhancement factor.[18] In the slow-light application, it is the steep slope of the refractive index that contributes the most to the group index. Thus, the relatively flat shift of the background refractive index plays a minor role. Also, the slope of the refractive index will first increase as the pump intensity increases. However, too

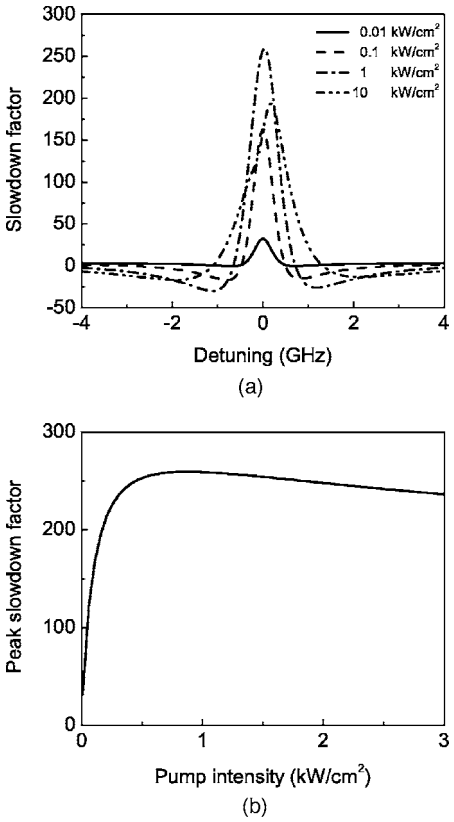

FIG. 5. The slowdown factor as a function of the pump-signal detuning and its peak value as a function of the pump intensity (a) A nonsymmetric spectrum of the slowdown factor occurs at a high pump intensity. This asymmetry arises because of the unevenly distributed energies and dipole moments of the transitions below and above the pump frequency. (b) There is an optimal pump intensity at which the slowdown factor is maximized. Beyond the optimal pump intensity, the peak slowdown factor decreases slowly as the pump intensity increases because transitions not in resonance with the pump frequency are hard to be saturated and broadened.

high an intensity will broaden the absorption dip and reduce the depth of the absorption dip. Therefore, from Fig. 4(b), we can see that the slope of the real part of the refractive index at a pump intensity of 10 kW/cm^2 is less than its counterpart at 1 kW/cm^2. There is an optimal pump intensity at which the peak slowdown factor is maximized.

Corresponding to the variations in Fig. 4(b), slowdown factors as a function of the signal-pump detuning under different pump intensities are shown in Fig. 5(a). As expected, the peak slowdown factor at a pump intensity of 10 kW/cm^2 is less than that at 1 kW/cm^2. The existence of a maximal peak slowdown factor can also be inferred from Fig. 5(b). A maximal peak slowdown factor is present at a pump intensity of about 0.75 kW/cm^2. From Fig. 5(a), an interesting point is that the spectrum of the slowdown factor at 10 kW/cm^2 is not completely symmetric with respect to the detuning and tilts toward the side of positive detuning. This asymmetry arises because the energies of the allowable transitions and corresponding dipole moments are not symmetrically distributed above and below the pump frequency. A symmetric Gaussian distribution in QD sizes does not lead to a symmetric Gaussian distribution in transition energy. Although the pump frequency is set to the transition frequency corresponding to the mean QD size, we can see from Fig. 3 that this pump frequency is not equal to the frequency at the peak absorption of this inhomogeneous-broadened QD system. At a high pump intensity, this asymmetry is clearly present in Fig. 5(a) because the distinctions between the saturations of different QDs are more obvious.

In Fig. 5(a), a peak slowdown factor of about a few hundreds is achievable under a reasonable pump intensity. The much smaller slowdown factor compared with that of the excitonic[3] PO in QWs are due to two factors. First, a much lower surface coverage ratio of QDs $[n_d\pi(\bar{s}^2+\sigma_s^2)=2.04\%]$ implies a poor overlap of the active medium with the optical field of the incident signal. Second, many transitions of QDs are not resonant with the pump frequency and cannot be efficiently utilized. An increase of the QD surface density and a more uniform QD growth will improve the slowdown factor in an inhomogeneously-broadened QD system significantly. Also, in contrast to the lower slowdown factor, the peak slowdown factor decreases more slowly as the pump intensity increases than the corresponding counterpart[6] in QWs. QDs with transition energies far away from the pump frequency are not efficiently utilized, but their absorption dips are not easily saturated and broadened, either. Thus, the drop of the peak slowdown factor with a high pump intensity is not so fast as in the case of QWs.

IV. CONCLUSION

We have investigated slow light using PO in an inhomogeneously-broadened QD system at a low temperature. Unlike slow light using EIT in a similar system where the inhomogeneous broadening of QDs may wash out the coherent effect, an absorption dip can be still present using coherent population oscillation in the absorption spectrum even though not all transitions are in resonance with the pump frequency. This absorption dip should be present at the bottom of a broad spectral hole at low temperatures and on an overall-saturated background absorption at the room temperature. A slowdown factor of a few hundred should be achievable at a low temperature for a normal-incidence geometry. Improvements of the surface density and uniformity of QDs can increase the slowdown factor.

ACKNOWLEDGMENTS

We are grateful for the technical discussion with Professor Connie J. Chang-Hasnain at University of California at Berkeley and Professor Hailin Wang at University of Oregon. This work is supported by DARPA under Grant No. AFSA3631-22549 and AFOSR under Grant No. AFUCALSA4455-32432PG.

APPENDIX A: THE VARIATIONAL APPROACH FOR EXCITON STATE IN A QUANTUM DOT

The inverse of the conduction band effective mass $\gamma_c(\mathbf{r}_e)$, the two Luttinger parameters $\gamma_1(\mathbf{r}_h)$ and $\gamma_2(\mathbf{r}_h)$, as well as the

QD confinement potentials $V_e(\mathbf{r}_e)$ and $V_h(\mathbf{r}_h)$ are position dependent and can be explicitly written as

$$\gamma_c(\mathbf{r}_e) = \gamma_{c,b} + (\gamma_{c,d} - \gamma_{c,b})\left[U\left(z_e + \frac{h}{2}\right) - U\left(z_e - \frac{h}{2}\right)\right] \times U(s - \rho_e),$$

$$\gamma_{1(2)}(\mathbf{r}_h) = \gamma_{1(2),b} + (\gamma_{1(2),d} - \gamma_{1(2),b}) \times \left[U\left(z_h + \frac{h}{2}\right) - U\left(z_h - \frac{h}{2}\right)\right]U(s - \rho_h),$$

$$V_{e(h)}(\mathbf{r}_{e(h)}) = -V_{e(h),b}\left[U\left(z_{e(h)} + \frac{h}{2}\right) - U\left(z_{e(h)} - \frac{h}{2}\right)\right] \times U(s - \rho_{e(h)}), \tag{A1}$$

where $U(z)$ is the Heaviside step function; $\gamma_{c,b}$ and $\gamma_{c,d}$ are the inverse of the effective masses in the barrier and dot region, respectively; $\gamma_{1(2),b}$ and $\gamma_{1(2),d}$ are the Luttinger's parameters in the barrier and dot regions; and $V_{e,b}$ as well as $V_{h,b}$ are the potential barriers for the electron and hole parts. Using Eqs. (1) and (2), we can write the expectation value $\langle\Psi_{ex}|H_{eh}|\Psi_{ex}\rangle$ as

$$\begin{aligned}\langle\Psi_{ex}|H_{eh}|\Psi_{ex}\rangle = {} & [\gamma_{c,b} + (\gamma_{c,d} - \gamma_{c,b})T^d_{\perp,e}(\lambda_e,s)]K^d_{z,e} + \gamma_{c,b}K^b_{z,e} \\ & + [\gamma_{z,b} + (\gamma_{z,d} - \gamma_{z,b})T^d_{\perp,h}(\lambda_h,s)]K^d_{z,h} \\ & + \gamma_{z,b}K^b_{z,h} + [\gamma_{c,b} + (\gamma_{c,d} - \gamma_{c,b})T^d_{z,e}] \\ & \times K^d_{\perp,e}(\lambda_e,s) + \gamma_{c,b}K^b_{\perp,e}(\lambda_e,s) \\ & + [\gamma_{\perp,b} + (\gamma_{\perp,d} - \gamma_{\perp,b})T^d_{z,h}]K^d_{\perp,h}(\lambda_h,s) \\ & + \gamma_{\perp,b}K^b_{\perp,h}(\lambda_h,s) - V_{e,b}T^d_{z,e}T^d_{\perp,e}(\lambda_e,s) \\ & - V_{h,b}T^d_{z,h}T^d_{\perp,h}(\lambda_h,s) \\ & - \frac{e^2}{4\pi\epsilon}\langle\Psi_{ex}|\frac{1}{|\boldsymbol{\rho}_e - \boldsymbol{\rho}_h|}|\Psi_{ex}\rangle,\end{aligned} \tag{A2}$$

where $\gamma_{z,b(d)}$ and $\gamma_{\perp,b(d)}$ are defined as

$$\gamma_{z,b(d)} = \gamma_{1,b(d)} - 2\gamma_{2,b(d)},$$

$$\gamma_{\perp,b(d)} = \gamma_{1,b(d)} + \gamma_{2,b(d)}, \tag{A3}$$

and various overlap integrals $T^d_{z,e}$, $T^d_{z,h}$, $T^d_{\perp,e}(\lambda_e,s)$, and $T^d_{\perp,h}(\lambda_h,s)$ as well as the kinetic integrals $K^d_{z,e}$, $K^d_{z,h}$, $K^d_{\perp,e}(\lambda_e,s)$, $K^d_{\perp,h}(\lambda_h,s)$, $K^b_{\perp,e}(\lambda_e,s)$, and $K^b_{\perp,h}(\lambda_h,s)$ are defined as

$$T^d_{z,e} = \langle\varphi_e|\left[U\left(z_e + \frac{h}{2}\right) - U\left(z_e - \frac{h}{2}\right)\right]|\varphi_e\rangle,$$

$$T^d_{z,h} = \langle\varphi_h|\left[U\left(z_h + \frac{h}{2}\right) - U\left(z_h - \frac{h}{2}\right)\right]|\varphi_h\rangle,$$

$$T^d_{\perp,e}(\lambda_e,s) = \langle\psi_e|U(s - \rho_e)|\psi_e\rangle,$$

$$T^d_{\perp,h}(\lambda_h,s) = \langle\psi_h|U(s - \rho_h)|\psi_h\rangle,$$

$$K^d_{z,e} = \langle\varphi_e|\frac{P_{z,e}[U(z_e + h/2) - U(z_e - h/2)]P_{z,e}}{2m_0}|\varphi_e\rangle,$$

$$K^d_{z,h} = \langle\varphi_e|\frac{P_{z,h}[U(z_h + h/2) - U(z_h - h/2)]P_{z,h}}{2m_0}|\varphi_h\rangle,$$

$$K^d_{\perp,e}(\lambda_e,s) = \langle\psi_e|\frac{\mathbf{P}_{\perp,e}\cdot U(s - \rho_e)\mathbf{P}_{\perp,e}}{2m_0}|\psi_e\rangle,$$

$$K^d_{\perp,h}(\lambda_h,s) = \langle\psi_h|\frac{\mathbf{P}_{\perp,h}\cdot U(s - \rho_h)\mathbf{P}_{\perp,h}}{2m_0}|\psi_h\rangle,$$

$$K^b_{\perp,e}(\lambda_e,s) = \langle\psi_e|\frac{\mathbf{P}_{\perp,e}\cdot U(\rho_e - s)\mathbf{P}_{\perp,e}}{2m_0}|\psi_e\rangle,$$

$$K^b_{\perp,h}(\lambda_h,s) = \langle\psi_h|\frac{\mathbf{P}_{\perp,h}\cdot U(\rho_h - s)\mathbf{P}_{\perp,h}}{2m_0}|\psi_h\rangle. \tag{A4}$$

The normalization of the individual electron part $\psi_e(\rho_e)$ and hole part $\psi_h(\rho_h)$ of the variational wave function $\Psi_{ex}(\mathbf{r}_e,\mathbf{r}_h)$ leads to the following expressions of the normalization constants $A(\lambda_e)$ and $A(\lambda_h)$:

$$A(\lambda_{e(h)}) = \frac{1}{\sqrt{36\pi}}\left(\frac{2\lambda_{e(h)}}{s}\right)^2. \tag{A5}$$

With this normalization condition, the corresponding expressions can be calculated explicitly using Eqs. (2) and (3) as follows:

$$T^d_{z,e} = |A_{z,e}|^2\left[\frac{h}{2} + \frac{\sin(k_e h)}{2k_e}\right],$$

$$T^d_{z,h} = |A_{z,h}|^2\left[\frac{h}{2} + \frac{\sin(k_h h)}{2k_h}\right],$$

$$T^d_{\perp,e}(\lambda_e,s) = 1 - \frac{1}{9}(4\lambda_e^3 + 14\lambda_e^2 + 18\lambda_e + 9)e^{-2\lambda_e},$$

$$T^d_{\perp,h}(\lambda_h,s) = 1 - \frac{1}{9}(4\lambda_h^3 + 14\lambda_h^2 + 18\lambda_h + 9)e^{-2\lambda_h},$$

$$K^d_{z,e} = \frac{\hbar^2 k_e^2}{2m_0}|A_{z,e}|^2\left[\frac{h}{2} - \frac{\sin(k_e h)}{2k_e}\right],$$

$$K^d_{z,h} = \frac{\hbar^2 k_h^2}{2m_0}|A_{z,h}|^2\left[\frac{h}{2} - \frac{\sin(k_h h)}{2k_h}\right],$$

$$K^d_{\perp,e}(\lambda_e,s) = \frac{\hbar^2}{36m_0}\left(\frac{2\lambda_e}{s}\right)^2 \times \left[\frac{3}{2} - \left(2\lambda_e^3 + 3\lambda_e^2 + 3\lambda_e + \frac{3}{2}\right)e^{-2\lambda_e}\right],$$

$$K^d_{\perp,h}(\lambda_h,s)=\frac{\hbar^2}{36m_0}\left(\frac{2\lambda_h}{s}\right)^2 \times\left[\frac{3}{2}-\left(2\lambda_h^3+3\lambda_h^2+3\lambda_h+\frac{3}{2}\right)e^{-2\lambda_h}\right],$$

$$K^b_{\perp,e}(\lambda_e,s)=\frac{\hbar^2}{36m_0}\left(\frac{2\lambda_e}{s}\right)^2\left(2\lambda_e^3+3\lambda_e^2+3\lambda_e+\frac{3}{2}\right)e^{-2\lambda_e},$$

$$K^b_{\perp,h}(\lambda_h,s)=\frac{\hbar^2}{36m_0}\left(\frac{2\lambda_h}{s}\right)^2\left(2\lambda_h^3+3\lambda_h^2+3\lambda_h+\frac{3}{2}\right)e^{-2\lambda_h}. \tag{A6}$$

The expectation value of the Coulomb potential is required in the calculation. We first decompose the Coulomb potential into a series containing the Bessel functions of the first kind

$$\frac{1}{|\boldsymbol{\rho}_e-\boldsymbol{\rho}_h|}=\sum_{m=-\infty}^{\infty}\int_0^\infty dk e^{im(\phi_e-\phi_h)}J_m(k\rho_e)J_m(k\rho_h). \tag{A7}$$

The expectation value of the Coulomb potential can be written as

$$\begin{aligned}\left\langle\Psi_{ex}\left|\frac{1}{|\boldsymbol{\rho}_e-\boldsymbol{\rho}_h|}\right|\Psi_{ex}\right\rangle &= \sum_{m=-\infty}^{\infty}\int_0^\infty dk\langle\Psi_{ex}|e^{im(\phi_e-\phi_h)}J_m(k\rho_e)J_m(k\rho_h)|\Psi_{ex}\rangle\\ &= \sum_{m=-\infty}^{\infty}\int_0^\infty dk\int_{-\pi}^{\pi}d\phi_e e^{im\phi_e}\int_{-\pi}^{\pi}d\phi_h e^{-im\phi_h}\int_0^\infty d\rho_e\rho_e J_m(k\rho_e)|A(\lambda_e)|^2\left(\rho_e+\frac{s}{\lambda_e}\right)^2\exp\left(-2\lambda_e\frac{\rho_e}{s}\right)\\ &\quad\times\int_0^\infty d\rho_h\rho_h J_m(k\rho_h)|A(\lambda_h)|^2\left(\rho_h+\frac{s}{\lambda_h}\right)^2\exp\left(-2\lambda_h\frac{\rho_h}{s}\right)\\ &= \left(\frac{\lambda_e^4}{18}\right)\left(\frac{\lambda_h^4}{18}\right)\int_0^\infty dk\int_0^\infty dx_e\left(x_e^3+\frac{4}{\lambda_e}x_e^2+\frac{4}{\lambda_e^2}\right)J_0\left(\frac{sx_e}{2}\right)e^{-\lambda_e x_e}\int_0^\infty dx_h\left(x_h^3+\frac{4}{\lambda_h}x_h^2+\frac{4}{\lambda_h^2}\right)J_0\left(\frac{sx_h}{2}\right)e^{-\lambda_h x_h}.\end{aligned} \tag{A8}$$

In Eq. (A8), we replace the power terms of the variables x_e and x_h as follows:

$$x_e^n\to(-1)^n\frac{\partial^n}{\partial\lambda_e^n},\quad x_h^n\to(-1)^n\frac{\partial^n}{\partial\lambda_h^n}. \tag{A9}$$

There is an analytical expression for the Laplace transformation of the zeroth-order Bessel function of the first kind

$$\int_0^\infty dx J_0(ax)e^{-bx}=\frac{1}{\sqrt{a^2+b^2}}. \tag{A10}$$

With Eqs. (A8)–(A10), the expectation value of the Coulomb potential can be written as

$$\begin{aligned}&\left\langle\Psi_{ex}\left|\frac{1}{|\boldsymbol{\rho}_e-\boldsymbol{\rho}_h|}\right|\Psi_{ex}\right\rangle\\ &=\left(\frac{2}{s}\right)\left(\frac{\lambda_e^4}{18}\right)\left(\frac{\lambda_h^4}{18}\right)\left(\frac{d^3}{d\lambda_e^3}-\frac{4}{\lambda_e}\frac{d^2}{d\lambda_e^2}+\frac{4}{\lambda_e^2}\frac{d}{d\lambda_e}\right)\\ &\quad\times\left(\frac{d^3}{d\lambda_h^3}-\frac{4}{\lambda_h}\frac{d^2}{d\lambda_h^2}+\frac{4}{\lambda_h^2}\frac{d}{d\lambda_h}\right)\int_0^\infty dt\frac{1}{\sqrt{\lambda_e^2+t^2}}\frac{1}{\sqrt{\lambda_h^2+t^2}}.\end{aligned} \tag{A11}$$

After carrying out these derivatives, Eq. (A11) is rewritten as

$$\left\langle\Psi_{ex}\left|\frac{1}{|\boldsymbol{\rho}_e-\boldsymbol{\rho}_h|}\right|\Psi_{ex}\right\rangle =\frac{\lambda_e^5\lambda_h^5}{18s}\int_0^\infty dt\frac{(6\lambda_e^2+t^2)(6\lambda_h^2+t^2)}{\left[\left(t^2+\frac{\lambda_e^2+\lambda_h^2}{2}\right)^2-\left(\frac{\lambda_e^2-\lambda_h^2}{2}\right)^2\right]^{7/2}}. \tag{A12}$$

By changing the integration variable t as

$$t=\sqrt{\frac{\lambda_e^2+\lambda_h^2}{2}}\tan\theta, \tag{A13}$$

the expectation value of the Coulomb potential can be expressed as a one-dimensional integration

$$\left\langle\Psi_{ex}\left|\frac{1}{|\boldsymbol{\rho}_e-\boldsymbol{\rho}_h|}\right|\Psi_{ex}\right\rangle=\frac{\lambda_e^5\lambda_h^5}{18s}\left(\frac{\lambda_e^2+\lambda_h^2}{2}\right)^{-13/2}F(\lambda_e,\lambda_h),$$

$$F(\lambda_e,\lambda_h)=\int_0^{\pi/2} d\theta \frac{\cos^8\theta}{\left[1-\left(\frac{\lambda_e^2-\lambda_h^2}{\lambda_e^2+\lambda_h^2}\right)^2\cos^4\theta\right]^{7/2}} \times\left[6\lambda_e^2\cos^2\theta+\left(\frac{\lambda_e^2+\lambda_h^2}{2}\right)\sin^2\theta\right] \times\left[6\lambda_h^2\cos^2\theta+\left(\frac{\lambda_e^2+\lambda_h^2}{2}\right)\sin^2\theta\right]. \quad \text{(A14)}$$

Equations (A6) and (A14) are then substituted into Eq. (A2) to obtain the parameters λ_e and λ_h which minimize the expectation value $\langle\Psi_{ex}|H_{eh}|\Psi_{ex}\rangle$. After the parameters λ_e and λ_h are determined, the overlap integral I_{ch} can be also calculated using the following analytical expression:

$$I_{ch}=\left\{2B_{z,e}B_{z,h}\frac{e^{-(\nu_e+\nu_h)h/2}}{\nu_e+\nu_h}+A_{z,e}A_{z,h} \times\left[\frac{\sin[(k_e+k_h)h/2]}{k_e+k_h}+\frac{\sin[(k_e-k_h)h/2]}{k_e-k_h}\right]\right\} \times\frac{8\lambda_e\lambda_h}{3(\lambda_e+\lambda_h)^2}\left[2\frac{\lambda_e\lambda_h}{(\lambda_e+\lambda_h)^2}+1\right]. \quad \text{(A15)}$$

APPENDIX B: THE LINEAR PERMITTIVITY TENSOR FOR POPULATION OSCILLATION IN QUANTUM DOTS

We label the quantities from Eqs. (5)–(8) by a label n to obtain the contribution from the n_{th} QD. Following a similar approach in Ref. 6, functions $H_n(\omega_p)$, $\Gamma^n_{s,\text{eff}}(\delta)$, $D_n(\omega_s,\omega_p)$, $F_n(\omega_s,\omega_p)$, and $G_n(\omega_s,\omega_p)$ for the n_{th} QD are defined to simplify the expression of the permittivity tensor:

$$H_n(\omega_p)=\frac{N_n^{(p)}-1}{\omega_p-\omega_{ex,n}+i\Gamma_{2,n}^{(p)}},$$

$$\Gamma^n_{s,\text{eff}}(\delta)=\frac{1}{2}\left[\Gamma_{s,n}+\gamma_{s,n}+\frac{(\Gamma_{s,n}-\gamma_{s,n})(\Gamma_{s,n}-\gamma_{s,n}-\gamma_n)}{i\delta-(\Gamma_{s,n}+\gamma_{s,n})}\right],$$

$$D_n(\omega_s,\omega_p)=2\left(\frac{1}{\omega_s-\omega_{ex,n}+i\Gamma_{2,n}^{(p)}}-\frac{1}{\omega_p-\omega_{ex,n}-i\Gamma_{2,n}^{(p)}}\right),$$

$$F_n(\omega_s,\omega_p)=\delta+i[\gamma_n+2\Gamma^n_{s,eff}(\delta)]+2|\Omega_{p,n}|^2 \times\left(\frac{1}{\omega_p-\delta-\omega_{ex,n}-i\Gamma_{2,n}^{(p)}}-\frac{1}{\omega_s-\omega_{ex,n}+i\Gamma_{2,n}^{(p)}}\right),$$

$$G_n(\omega_s,\omega_p)=-\Gamma^n_{s,\text{eff}}(\delta)+2\gamma_{2,n}|\Omega_{p,n}|^2 \times\left[\frac{N_n^{(p)}-1}{(\omega_p-\delta-\omega_{ex,n}-i\Gamma_{2,n}^{(p)})(\omega_p-\omega_{ex,n}-i\Gamma_{2,n}^{(p)})}+\frac{N_n^{(p)}-1}{(\omega_s-\omega_{ex,n}+i\Gamma_{2,n}^{(p)})(\omega_p-\omega_{ex,n}+i\Gamma_{2,n}^{(p)})}\right], \quad \text{(B1)}$$

where $\delta=\omega_s-\omega_p$ is the signal-pump detuning; and $N_n^{(p)}$ and $\Gamma_{2,n}^{(p)}$ are the total populations in the conduction band and the dephasing constant for the n_{th} QD in the presence of the pump. The linear relative permittivity tensor $\bar{\epsilon}_s^L(\omega_s)$ is the sum of the contribution from each QD

$$\bar{\epsilon}_s^L(\omega_s)=\begin{pmatrix}\epsilon_{bgd}&0\\0&\epsilon_{bgd}\end{pmatrix}+\sum_n\frac{\pi s_n^2}{A}\frac{|I_{ch,n}er_{ch}|^2}{2\hbar\epsilon_0V_{ol,n}}\frac{2(N_n^{(p)}-1)}{\omega_s-\omega_{ex,n}+i\Gamma_{2,n}^{(p)}} \begin{pmatrix}1+\frac{|\Omega_{p,n}|^2D_n(\omega_s,\omega_p)(1-2i\gamma_{2,n})H_n(\omega_p)}{F_n(\omega_s,\omega_p)+2iG(\omega_s,\omega_p)}&0\\0&1+\frac{|\Omega_{p,n}|^2D_n(\omega_s,\omega_p)}{F_n(\omega_s,\omega_p)}\end{pmatrix}, \quad \text{(B2)}$$

where ϵ_{bgd} is the background relative permittivity function; $V_{ol,n}=\pi s_n^2h$ is the volume of the particular QD; A is the area of the QD layer; and the ratio of $\pi s_n^2/A$ comes from the confinement of the light field transverse to the growth direction. In Eq. (B2), the first diagonal term represents the linear relative permittivity experienced by the signal with the same polarization as that of the pump. This polarization direction is denoted as $\hat{x}$. Similarly, the second diagonal component represents the linear relative permittivity experienced by the signal with a polarization orthogonal to that of the pump. The corresponding polarization direction is denoted as $\hat{y}$. We will replace the summation over n in Eq. (B2) with an integration over the radius s weighted by the probability distribution $f(s)$ of the radius s. Various functions and parameters in Eq. (B1) are then parametrized by the radius s. This is simply done by replacing the dependence on the dot label n by the dependence on the QD radius s. The susceptibility functions $\chi_x(\omega_s,s)$ and $\chi_y(\omega_s,s)$ are generalized from the expression in Eq. (B2) as follows:

$$\frac{|I_{ch,n}er_{ch}|^2}{2\hbar\epsilon_0V_{ol,n}}\frac{2(N_n^{(p)}-1)}{\omega_s-\omega_{ex,n}+i\Gamma_{2,n}^{(p)}}\left(1+\frac{|\Omega_{p,n}|^2D_n(\omega_s,\omega_p)(1-2i\gamma_{2,n})H_n(\omega_p)}{F_n(\omega_s,\omega_p)+2iG(\omega_s,\omega_p)}\right)\rightarrow\chi_x(\omega_s,s),$$

$$\frac{|I_{ch,n}er_{ch}|^2}{2\hbar\epsilon_0V_{ol,n}}\frac{2(N_n^{(p)}-1)}{\omega_s-\omega_{ex,n}+i\Gamma_{2,n}^{(p)}}\left(1+\frac{|\Omega_{p,n}|^2D_n(\omega_s,\omega_p)}{F_n(\omega_s,\omega_p)}\right)\rightarrow\chi_y(\omega_s,s). \quad \text{(B3)}$$

The expressions in Eq. (B3) can be substituted into Eq. (10) to obtain the linear relative permittivity experienced by the signal. For the parallel polarization configuration, the absorption dip obtained from the susceptibility $\chi_x(\omega_s, s)$ is significant since the populations of the two spin subsystems oscillate in phase and will not cancel each other.[6] On the other hand, for the orthogonal polarization configuration, the out-of-phase oscillations will cancel each other and no significant absorption dip can be obtained from the susceptibility $\chi_y(\omega_s, s)$. Thus, for slow light based on PO using excitons of QDs with inhomogeneous broadening, the parallel-polarization configuration should be used.

*Corresponding author. Electronic address: s-chuang@uiuc.edu

[1] L. V. Hau, S. E. Harris, Z. Dutton, and C. H. Behroozi, Nature (London) **397**, 594 (1999).
[2] M. S. Bigelow, N. N. Lepeshkin, and R. W. Boyd, Phys. Rev. Lett. **90**, 113903 (2003).
[3] P. C. Ku, F. Sedgwick, C. J. Chang-Hasnain, P. Palinginis, T. Li, H. Wang, S. W. Chang, and S. L. Chuang, Opt. Lett. **29**, 2291 (2004).
[4] T. Li, H. Wang, N. H. Kwong, and R. Binder, Opt. Express **11**, 3298 (2003).
[5] E. Podivilov, B. Sturman, A. Shumelyuk, and S. Odoulov, Phys. Rev. Lett. **91**, 083902 (2003).
[6] S. W. Chang, S. L. Chuang, P. C. Ku, C. J. Chang-Hasnain, P. Palinginis, and H. Wang, Phys. Rev. B **70**, 235333 (2004).
[7] J. Kim, S. L. Chuang, P. C. Ku, and C. J. Chang-Hasnain, J. Phys.: Condens. Matter **16**, S3727 (2004).
[8] U. Woggon, S. Gaponenko, W. Langbein, A. Uhrig, and C. Klingshirn, Phys. Rev. B **47**, 3684 (1993).
[9] Y. Masumoto, T. Kawazoe, and T. Yamamoto, Phys. Rev. B **52**, 4688 (1995).
[10] N. Sakakura and Y. Masumoto, Phys. Rev. B **56**, 4051 (1997).
[11] Y. Sugiyama, Y. Nakata, and T. Futatsugi, Fujitsu Sci. Tech. J. **34**, 182 (1998).
[12] J. J. Sakurai, *Modern Quantum Mechanics*, Revised ed. (Addison-Wesley, Reading, MA, 1994).
[13] P. K. Kondratko, S. L. Chuang, G. Walter, N. Holonyak Jr., R. D. Heller, X. B. Zhang, and R. D. Dupuis, IEEE Photonics Technol. Lett. **17**, 938 (2005).
[14] H. Wang, K. Ferrio, D. G. Steel, Y. Z. Hu, R. Binder, and S. W. Koch, Phys. Rev. Lett. **71**, 1261 (1993).
[15] M. Sugawara, H. Ebe, N. Hatori, M. Ishida, Y. Arakawa, T. Akiyama, K. Otsubo, and Y. Nakata, Phys. Rev. B **69**, 235332 (2004).
[16] G. G. Van de Walle, Phys. Rev. B **39**, 1871 (1989).
[17] A. Yariv, *Quantum Electronics*, 3rd ed. (John Wiley and Sons, New York, 1989).
[18] C. H. Henry, IEEE J. Quantum Electron. **18**, 259 (1982).